

Oil & Natural Gas Technology

DOE Award No.: DE-FE0013531

Quarterly Research Performance Progress Report (Period ending 12/31/2014)

**Assessing the response of methane hydrates to environmental
change at the Svalbard continental margin**
Project Period (11/1/2013 to 10/31/2016)

Submitted by:
Marta E. Torres



Oregon State University
DUNS #: 053599908
104 COAS Admin. Bldg.
Corvallis, OR 97331-5503
e-mail: mtorres@coas.oregonstate.edu
Phone number: (541) 737-2902

Prepared for:
United States Department of Energy
National Energy Technology Laboratory



Office of Fossil Energy

EXECUTIVE SUMMARY

In November 2013, Oregon State University initiated the project entitled: **Assessing the response of methane hydrates to environmental change at the Svalbard continental margin.** In this project, we will take advantage of a unique opportunity to collect samples from the Svalbard continental margin. The overall objective of this research is to constrain the biogeochemical response of the gas hydrate system on the Svalbard margin to environmental change. The locations sampled shall provide key datasets that allow examination of the system with respect to sediment temperature fluctuations driven by thermal changes in the overlying water column and by hydrothermal circulation in the sediments. Because of a delay in the planned expedition, we reconfigured the program based on discussions with NETL program managers and submitted a revised SOPO. In the new plan, we will collect samples in two expeditions, the first of which happened Oct 7-21, 2014. However because of delays setting the project continuation going, we have not been able to make much progress the period from November 14 onwards. As we get the new revised contract in place, we can continue with the project

PROGRESS, RESULTS, AND DISCUSSION

1. Expedition(s) update

- a. The cruise to Vestnesa Ridge on the Norwegian RV Helmer Hanssen cruise took place from 7th to the 18th of October. We will be able to conduct the geochemistry and microbiology tasks of the DOE funded project on that region, i.e., sampling across a transect with different levels of methane flux. WeiLi Hong sailed on this cruise and collected the pore water and sediment chemistry. Norwegian scientist Friederike Gründger collected samples for microbiology. The Arctic University of Norway (CAGE Center) provided some shipboard supplies (e.g. reagents, liquid nitrogen, core handling equipment, etc.). Additional supplies needed for the expedition were sent from Bremen, or were hand-carried by WeiLi Hong from OSU. A short summary of the sites visited and cores recovered is given in the Appendix. Unfortunately because of weather problems (extensive sea ice coverage in October) and problems with the winch, only short cores were retrieved. We believe that two of the cores sampled a near-seep since there is a slight decrease in sulfate (to 20 mM), but penetration was limited. Because of these issues another expedition is planned for May 16-29 also on the Norwegian RV Helmer Hanssen. For this expedition the Norwegian scientists have secured the use of a towed-camera to observe the seafloor and better position the cores. I expect a much better sample collection from this expedition.
- b. We are still planning on participating on the German RV Heincke from 30 July to 25 September to collect samples aided by a remotely operated vehicle (ROV), as well as conduct the water column aspects of the project. The RV Heincke's original task for this expedition is to deploy and test a new AUV system under development. However Prof. Bohrmann has agreed to allocate 35% of the ship-time for me to conduct the DOE-related tasks.

2. Instrument update-

- a. The Green House analyzer is now totally functional, and the procedures/methodologies/calibration for use at sea are full established. We are developing a manuscript describing the use/application and reliability of this instrument. The instrument is being shipped back to the US, since the export permit

(Carnet) expires after a year. We will resend the equipment for participation in the upcoming cruises off Svalbard in May and July to map water column methane.

3. Microbiology.
 - a. Microbial community characterization depends on extraction, amplification, and sequencing of DNA from environmental samples. Commonly used DNA extraction kits may represent a source of contamination¹ and do not lyse all cells equally, potentially resulting in a biased community analysis that is particularly relevant when analyzing low-biomass samples. Methods of DNA extraction use CTAB for cell lysis followed by a chloroform extraction and DNA precipitation, or DNA extraction kits with minor protocol adjustments. Newer methods developed for marine sediments include separate extraction of intracellular and extracellular DNA, and a hot-alkaline extraction to lyse archaeal cell walls.
 - b. To date we have obtained low DNA yields (>200 ng DNA/g sediment) from all these extraction methods. 16S PCR of community DNA did not result in amplification across a range of template DNA concentrations (1-30 ng/reaction). The addition of PVPP to bind PCR inhibitors did not yield amplifiable DNA. Similarly, ethanol precipitations did not clean and concentrate DNA enough for amplification.
 - c. Further efforts to extract and amplify DNA will involve PCR of serial dilutions of template DNA to determine whether inhibition will still occur. We anticipate scaling up the amount of sediment used for extractions to 5-10 g and filter-concentrating DNA. A DNA polymerase capable of amplification under high humic acid and PCR inhibitor concentrations will also be used. Fluorescence in-situ hybridization (FISH) will be used to obtain cell densities if these relatively minor protocol adjustments fail to produce amplifiable DNA from Svalbard continental margin sediments.
4. Modeling- We have continued making progress towards providing a numerical model perspective of methane hydrate stability and saturation in the Ulleung Basin. Status of that work is given in Appendix 2

PROBLEMS OR DELAYS

We encountered a significant set-back when the planned expedition in the R/V M.S. Merian got cancelled due to massive engine failure of the vessel. We immediately notified the program management and set up a set of conference calls to decide the best options to move forward. This was resolved by participating on two expeditions (October 2014, July-September 2015). Unfortunately the October expedition only resulted in a few cores that reached the depth of interest (SMTZ).. We will re-core the area during another expedition this coming May, for a total of three expeditions to the region during the project duration.

PRODUCTS

- Report on sample collection during R/V Hansen expedition, and analytical results
- Report on Numerical Simulations

RV Helmer Hanssen

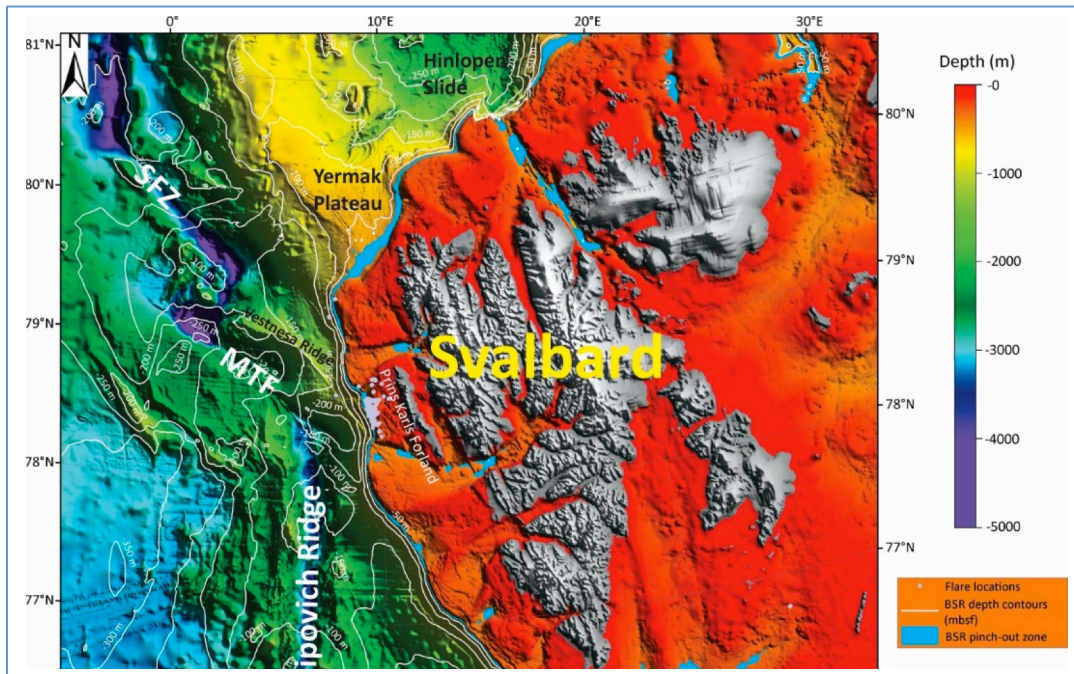
07. 10. 2014 – 18. 10. 2014

Methane venting and gas hydrates off west coast of Svalbard



Note- This is a Norwegian expedition, under the auspices of CAGE, we summarize here the information relevant to the sediment sampling to be used in support of the DOE project

The cruise targeted the climate-sensitive area outside Svalbard (Figure 1). The stations visited for sediment/pore water sample collection during the October 2014 expedition of the RV Hansen are shown in Figure 2.



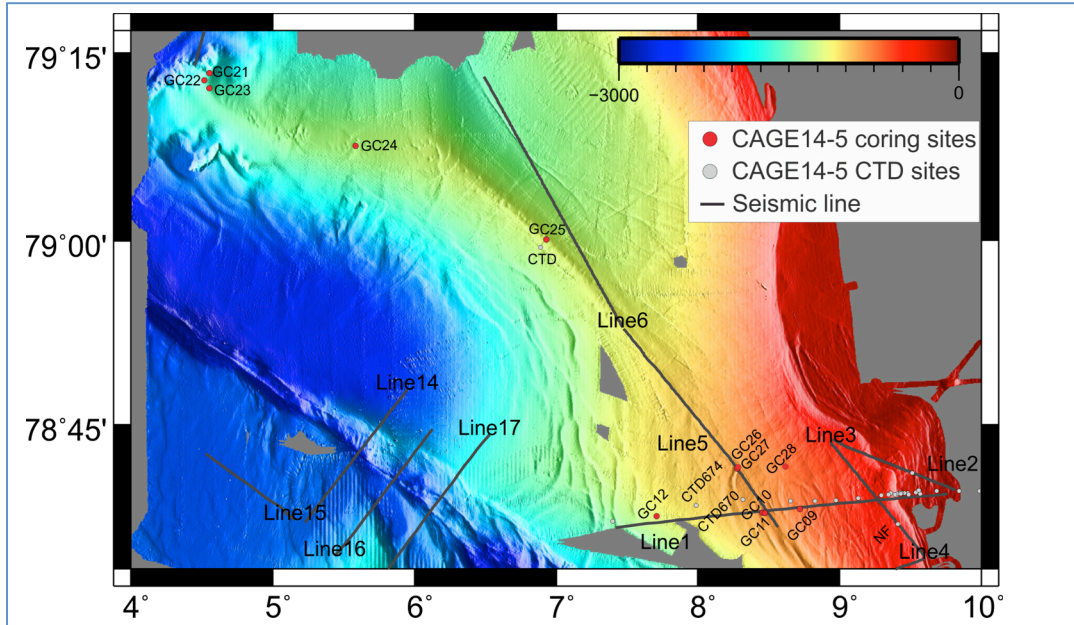
The cruise primarily aimed at collect field data in the area of the West-Spitsbergen continental margin (Figure 1) that will allow investigating the gas hy-

drate dynamics. Our objectives are:

- To evaluate stability conditions of the gas hydrates based on the analysis of the geo-chemical compositions and temperature lance measurements.
- To obtain a better understanding of stratigraphic development and sedimentation rate on the Vestnesa Ridge.
- To obtain baseline information on fluid expulsion processes on the Vestnesa Ridge which allow an optimized design of a planned seafloor observatory to be deployed in this area.

Geochemistry/Microbiology program

The goals of this program were to collect water and sediment core samples from a high latitude setting (the Svalbard Margin) across gradients where methane hydrates show vulnerability to environmental change. Samples will be used for chemical and microbiological analyses to assess changes in chemistry and microbiology that constrain the biogeochemical response at locations where methane hydrates are sensitive to environmental change.



During this expedition we visited 14 sites, as shown in Table 1.

Each of these we took 10 cm whole round samples for microbiology (both OSU and

UiT labs.), the adjacent 20-30 cm sections were sampled for pore water analyses using rhizons. In all cases the samples were maintained at in situ temperatures of <1C. Head-

Table 1- Gravity cores collected during CAGE-14 expedition

	GC03	GC07	GC08	GC09	Strong H ₂ S smell		GC12
					GC10	GC11	
WD (m)	236	246	245	716	870	870	1186
Core length (cm)	64	77	29	184	84	134	260
# of pore water samples	1	3	2	10	8	9	17
# of Mbio samples	1	2		6		4	8
	GC21	GC23	GC24	GC25	GC26	GC27	GC28
WD (m)	1650	1554	1308	1209	888	881	
Core length (cm)	73	268	270	260	241	215	198
# of pore water samples	4	14	18	18	17	14	8
# of Mbio samples		9		7	6	6	

space samples were taken from the pore water whole round section and stored at 4C.

Table 2. PW protocol

- 50 uL for salinity
- 3 mL for $d^{13}C$ of DIC (1.5 mL each vials, duplicates for CAGE, with 10 mL $HgCl_2$)
- 1.5 mL for SO_4 conc. (with 0.1 mL ZnAc)
- 1.5 mL for Cl conc.
- 1.5 mL for DIC concentration (with 10 mL $HgCl_2$)
- 3 mL for nutrient
- 2-3 mL for cation

A total of 143 pore fluid samples were collected, processed as shown in Table 2, and stored for shore-based analyzes. To date the samples have been analyzed for major cations and sulfur (sulfate). Data is listed in Table 3, and shows that most samples still contain sulfate, and thus the SMTZ was not reached. Because we deemed these samples not suitable to address the project objectives, we will only analyze a small subset of these for isotope work. We expect to collect a better suite of samples in the next expedition (May 2015).

A total of 49 whole-round samples were collected for microbiology, and processed for FISH/DNA analyses immediately after collection. To date we have obtained low DNA yields (>200 ng DNA/g sediment) from all these extraction methods. 16S PCR of community DNA did not result in amplification across a range of template DNA concentrations (1-30 ng/reaction). The addition of PVPP to bind PCR inhibitors did not yield amplifiable DNA. Similarly, ethanol precipitations did not clean and concentrate DNA enough for amplification. Further efforts to extract and amplify DNA will involve PCR of serial dilutions of template DNA to determine whether inhibition will still occur. We anticipate scaling up the amount of sediment used for extractions to 5-10 g and filter-concentrating DNA. A DNA polymerase capable of amplification under high humic acid and PCR inhibitor concentrations will also be used. Fluorescence in-situ hybridization (FISH) will be used to obtain cell densities if these relatively minor protocol adjustments fail to produce amplifiable DNA from Svalbard continental margin sediments

Table 3- Pore water analyses from CAGE-14 cruise

Run Date	Core/Site	Depth (cm)		Na (mmol/L)	±	Mg (mmol/L)	±	K (mmol/L)	±	Ca (mmol/L)	±	Sr (µmol/L)	±	S (mmol/L)	±
12/15/14	853-07	19		466	5	52.7	0.7	11.4	0.3	10.1	0.2	78	6	26.6	0.6
12/15/14	853-07	55.5		472	6	53.8	0.8	11.5	0.3	10.5	0.2	80	7	27.8	0.6
12/15/14	854-08	8.5		468	7	53.6	1.0	11.3	0.3	10.4	0.2	80	7	28.1	0.6
12/15/14	854-08	18.5		454	5	51.6	0.8	11.5	0.3	9.9	0.2	77	7	26.6	0.6
12/15/14	855-09	14.5		476	5	52.8	0.5	11.9	0.3	9.9	0.2	79	6	26.0	0.6
12/15/14	855-09	23		471	6	53.6	1.0	11.7	0.3	10.4	0.2	80	6	27.7	0.6
12/15/14	855-09	47		472	4	53.0	0.5	11.7	0.3	10.2	0.2	79	6	27.6	0.6
12/15/14	855-09	55		469	4	52.5	0.8	11.4	0.3	10.1	0.2	79	7	26.6	0.7
12/15/14	855-09	76		462	5	51.4	0.6	11.3	0.2	9.8	0.2	78	6	25.8	0.6
12/15/14	855-09	106.5		470	5	51.5	0.8	11.6	0.3	9.8	0.2	81	6	25.5	0.6
12/15/14	855-09	115		465	8	51.2	0.9	11.4	0.3	9.7	0.2	79	7	25.5	0.5
12/15/14	855-09	136.5		465	6	50.7	0.8	11.4	0.3	9.6	0.2	80	7	25.4	0.7
12/15/14	855-09	165.5		471	6	51.2	0.7	11.5	0.4	9.4	0.2	79	6	24.8	0.6
12/15/14	856-10	10		465	5	52.2	0.6	11.4	0.2	9.8	0.2	79	6	26.8	0.6
12/15/14	856-10	20		467	7	52.6	0.8	11.2	0.3	9.1	0.2	78	6	24.6	0.6
12/15/14	856-10	30		469	5	52.3	0.6	11.4	0.2	8.7	0.2	77	6	24.1	0.7
12/15/14	856-10	40		472	6	52.5	0.8	11.5	0.3	8.2	0.2	77	7	23.1	0.7
12/15/14	856-10	50		481	5	53.4	0.9	11.8	0.3	7.6	0.2	78	6	23.6	0.6
12/15/14	856-10	60		474	6	52.2	0.6	11.4	0.3	6.8	0.2	74	6	21.4	0.6
12/15/14	856-10	70		473	4	51.8	0.6	11.5	0.3	6.1	0.2	73	6	21.3	0.6
12/15/14	856-10	80		471	6	51.0	0.6	11.4	0.3	5.6	0.2	71	6	20.9	0.7
12/15/14	857-11	18.5		473	4	53.2	0.7	11.6	0.3	10.4	0.2	80	6	28.2	0.5
12/15/14	857-11	26		494	14	55.5	1.7	12.0	0.3	10.8	0.4	85	7	29.7	1.1
12/15/14	857-11	48.5		469	7	52.6	1.0	11.6	0.3	10.0	0.2	79	7	27.5	0.6
12/16/14	857-11	48.5	(rpt)	477	3	53.2	0.6	11.9	0.3	10.1	0.1	76	5	27.0	0.3
12/15/14	857-11	56.5		473	4	53.1	0.6	11.6	0.3	10.0	0.2	80	6	27.8	0.6
12/15/14	857-11	80		470	5	52.7	0.8	11.5	0.2	9.8	0.2	78	6	27.9	0.6
12/15/14	857-11	87.5		473	5	53.1	0.7	11.6	0.2	9.8	0.2	79	6	27.4	0.6
12/16/14	857-11	87.5	(rpt)	479	3	53.3	0.6	11.8	0.3	9.9	0.1	76	5	26.5	0.5

Table 3- Pore water analyses from CAGE-14 cruise

Run Date	Core/Site	Depth (cm)		Na (mmol/L)	±	Mg (mmol/L)	±	K (mmol/L)	±	Ca (mmol/L)	±	Sr (µmol/L)	±	S (mmol/L)	±
12/15/14	857-11	109		471	7	53.0	0.8	11.6	0.3	9.5	0.2	78	6	28.6	0.6
12/15/14	857-11	118		476	7	53.3	0.7	11.6	0.3	9.6	0.2	78	6	28.7	0.6
12/15/14	857-11	126		477	5	53.2	0.9	12.0	0.3	9.4	0.2	77	7	25.4	0.6
12/16/14	857-11	126	(rpt)	478	3	53.2	0.6	12.1	0.2	9.3	0.1	73	5	24.6	0.4
12/15/14	858-12	15.5		478	5	53.9	0.9	11.8	0.3	10.7	0.2	82	7	28.2	0.6
12/15/14	858-12	24		466	4	52.1	0.6	11.4	0.3	10.4	0.2	79	6	28.1	0.6
12/15/14	858-12	47		469	6	53.1	0.7	11.4	0.3	10.5	0.2	80	6	28.1	0.5
12/16/14	858-12	47	(rpt)	473	4	53.1	0.6	11.5	0.2	10.5	0.1	77	5	27.5	0.4
12/15/14	858-12	54.5		472	5	53.7	0.6	11.2	0.3	10.6	0.2	81	6	27.9	0.6
12/15/14	858-12	77.5		472	5	53.0	0.7	11.5	0.3	10.5	0.2	81	6	27.6	0.6
12/15/14	858-12	84.5		476	6	53.4	0.7	11.7	0.3	10.5	0.2	81	6	27.8	0.6
12/16/14	858-12	84.5	(rpt)	478	3	53.2	0.6	11.9	0.2	10.5	0.1	78	5	27.2	0.2
12/15/14	858-12	106		471	5	52.2	0.6	11.6	0.3	10.2	0.2	80	6	27.3	0.6
12/15/14	858-12	114		474	5	52.8	0.6	11.6	0.3	10.3	0.2	80	6	27.1	0.6
12/15/14	858-12	136		476	7	53.2	1.0	11.5	0.4	10.3	0.2	81	7	26.9	0.7
12/16/14	858-12	136	(rpt)	480	3	53.2	0.6	11.7	0.2	10.3	0.1	77	5	26.3	0.5
12/15/14	858-12	144.5		476	7	53.1	0.7	11.6	0.3	10.3	0.2	80	7	26.7	0.6
12/15/14	858-12	166.5		477	5	53.4	0.5	11.3	0.3	10.3	0.2	80	6	26.6	0.6
12/15/14	858-12	174		469	4	52.2	0.6	11.1	0.2	10.0	0.2	78	6	26.0	0.6
12/16/14	858-12	174	(rpt)	472	5	52.5	0.8	11.4	0.2	10.0	0.2	75	5	25.1	0.3
12/15/14	858-12	196.5		474	5	52.8	0.9	11.4	0.4	10.1	0.2	79	7	25.9	0.5
12/15/14	858-12	204.5		469	4	52.0	0.8	11.2	0.3	9.9	0.2	78	6	25.1	0.5
12/15/14	858-12	227		474	5	52.5	0.6	11.2	0.2	9.9	0.2	79	6	25.1	0.6
12/16/14	858-12	227	(rpt)	477	4	52.9	0.7	11.5	0.2	9.9	0.1	77	5	24.3	0.3
12/15/14	858-12	234		475	5	52.1	0.6	11.4	0.3	9.8	0.2	78	6	24.9	0.6
12/15/14	867-21	27		477	5	54.9	0.6	11.0	0.2	10.9	0.2	81	6	28.6	0.6
12/15/14	867-21	37		477	5	54.5	0.6	10.9	0.3	10.7	0.2	80	6	28.4	0.6
12/16/14	867-21	37	(rpt)	478	3	54.0	0.7	11.1	0.2	10.6	0.1	77	5	27.4	0.2
12/15/14	867-21	51		476	6	54.3	0.7	11.0	0.3	10.7	0.2	80	6	28.4	0.7
12/15/14	867-21	63		472	4	54.0	0.5	10.7	0.3	10.6	0.2	79	6	28.0	0.7

Table 3- Pore water analyses from CAGE-14 cruise

Run Date	Core/Site	Depth (cm)	Na (mmol/L)	±	Mg (mmol/L)	±	K (mmol/L)	±	Ca (mmol/L)	±	Sr (µmol/L)	±	S (mmol/L)	±
12/15/14	869-23	20	475	6	53.4	0.7	10.9	0.3	10.0	0.2	79	7	26.0	0.6
12/16/14	869-23	23.5	463	4	53.5	0.6	10.5	0.2	10.5	0.1	76	5	27.9	0.3
12/16/14	869-23	47	465	4	53.7	0.7	10.6	0.2	10.6	0.1	77	5	27.9	0.3
12/16/14	869-23	56	467	5	53.7	0.7	10.7	0.2	10.6	0.1	76	5	27.7	0.3
12/16/14	869-23	75	466	4	53.5	0.6	10.8	0.4	10.4	0.1	76	5	27.5	0.3
12/16/14	869-23	83	464	4	53.3	0.7	10.6	0.4	10.3	0.1	76	5	27.2	0.4
12/16/14	869-23	155	466	5	53.6	0.6	10.7	0.2	10.6	0.1	77	5	27.8	0.3
12/16/14	869-23	178	468	3	52.9	0.7	10.6	0.2	9.8	0.1	75	5	25.5	0.4
12/16/14	869-23	210	465	4	52.5	0.6	10.6	0.2	9.6	0.1	74	5	25.2	0.3
12/16/14	869-23	225.5	468	3	52.7	0.6	10.6	0.1	9.6	0.1	74	5	24.9	0.3
12/16/14	869-23	234.5	467	5	52.6	0.6	10.4	0.2	9.6	0.1	74	5	24.7	0.3
12/16/14	870-24	15	465	3	53.5	0.7	10.8	0.2	10.5	0.1	77	5	27.5	0.6
12/16/14	870-24	34	467	3	53.5	0.6	10.7	0.2	10.5	0.1	77	5	27.1	0.5
12/16/14	870-24	56	468	6	53.5	0.6	10.7	0.3	10.4	0.1	77	5	26.7	0.3
12/16/14	870-24	66	472	5	53.8	0.6	10.7	0.3	10.5	0.1	77	5	26.6	0.3
12/16/14	870-24	75	473	5	53.8	0.6	10.9	0.3	10.4	0.1	78	5	26.4	0.4
12/16/14	870-24	95	470	4	53.4	0.6	10.8	0.2	10.3	0.1	77	5	25.6	0.4
12/16/14	870-24	105	471	3	53.5	0.8	10.8	0.2	10.4	0.1	77	5	25.7	0.5
12/16/14	870-24	115	472	3	53.4	0.6	10.8	0.2	10.2	0.1	77	5	25.3	0.3
12/16/14	870-24	137	471	3	53.2	0.6	10.8	0.3	10.3	0.1	77	5	24.9	0.3
12/16/14	870-24	146	440	3	50.1	0.6	10.1	0.2	9.6	0.1	70	5	23.2	0.5
12/16/14	870-24	155	447	3	50.7	0.6	10.4	0.2	9.7	0.1	71	5	23.7	0.2
12/16/14	870-24	174	477	3	53.8	0.7	10.9	0.3	10.4	0.1	77	5	24.7	0.5
12/16/14	870-24	183	470	6	53.1	0.6	10.7	0.2	10.2	0.1	76	5	24.5	0.2
12/16/14	870-24	193	473	4	53.4	0.7	10.8	0.2	10.3	0.1	76	5	24.4	0.2
12/16/14	870-24	218	472	6	53.5	0.7	10.7	0.3	10.2	0.1	76	5	24.0	0.4
12/16/14	870-24	228	449	4	50.7	0.6	10.3	0.2	9.6	0.1	71	5	22.5	0.3
12/16/14	870-24	237	475	4	53.7	0.8	10.9	0.2	10.3	0.2	76	5	23.9	0.3
12/16/14	870-24	257	473	3	53.2	0.6	10.8	0.2	10.2	0.1	76	5	23.7	0.4
12/16/14	871-25	18	475	3	54.0	0.6	11.3	0.3	10.8	0.1	78	5	28.3	0.3
12/16/14	871-25	26.5	471	3	53.4	0.7	11.0	0.2	10.6	0.1	77	5	28.0	0.3

Table 3- Pore water analyses from CAGE-14 cruise

Run Date	Core/Site	Depth (cm)	Na (mmol/L)	±	Mg (mmol/L)	±	K (mmol/L)	±	Ca (mmol/L)	±	Sr (µmol/L)	±	S (mmol/L)	±
12/16/14	871-25	34	470	7	53.4	0.7	11.0	0.2	10.5	0.1	76	5	27.4	0.3
12/16/14	871-25	57	468	4	53.1	0.6	10.9	0.2	10.4	0.1	75	5	27.1	0.4
12/16/14	871-25	72.5	475	5	53.5	0.6	11.1	0.2	10.4	0.2	77	5	26.9	0.2
12/16/14	871-25	108.5	477	3	53.8	0.6	11.0	0.2	10.3	0.1	77	5	26.2	0.4
12/16/14	871-25	116	473	6	53.2	0.6	10.8	0.3	10.1	0.1	76	5	25.8	0.5
12/16/14	871-25	136	472	6	52.9	0.7	10.9	0.3	9.9	0.1	75	5	25.3	0.2
12/16/14	871-25	148	470	3	52.5	0.6	10.9	0.3	9.8	0.1	74	5	24.9	0.5
12/16/14	871-25	156	469	5	52.4	0.9	10.8	0.2	9.8	0.1	74	5	24.4	0.2
12/16/14	871-25	160	474	3	53.0	0.6	11.1	0.2	10.2	0.1	76	5	26.1	0.3
12/16/14	871-25	177.5	473	3	52.8	0.6	10.9	0.2	9.7	0.1	75	5	24.1	0.3
12/16/14	871-25	188	470	4	52.2	0.6	10.8	0.2	9.6	0.1	74	5	23.7	0.2
12/16/14	871-25	198	472	3	52.3	0.6	10.9	0.2	9.5	0.1	74	5	23.6	0.3
12/16/14	871-25	218	465	5	51.5	0.7	10.7	0.2	9.3	0.1	73	5	23.0	0.3
12/16/14	871-25	228	473	5	52.6	0.6	10.9	0.3	9.5	0.1	74	5	22.8	0.3
12/16/14	871-25	234	476	3	52.6	0.6	11.1	0.3	9.4	0.1	74	5	22.7	0.3
12/16/14	871-25	256.5	473	5	52.3	0.7	10.9	0.3	9.3	0.1	74	5	22.1	0.4
12/15/14	872	23	459	4	52.8	0.7	10.8	0.3	10.2	0.2	80	6	27.1	0.5
12/15/14	872	34	424	4	48.9	0.7	10.1	0.2	9.4	0.2	73	6	25.1	0.6
12/15/14	872	40	456	6	52.5	0.6	10.9	0.3	10.1	0.2	80	6	27.2	0.5
12/15/14	872	60	459	5	52.5	0.6	11.0	0.3	10.1	0.2	80	6	27.2	0.5
12/15/14	872	71	463	5	53.0	0.6	11.0	0.2	10.2	0.2	81	6	27.2	0.6
12/15/14	872	80	459	5	52.2	0.7	11.0	0.2	10.1	0.2	79	6	27.2	0.6
12/15/14	872	103.5	459	5	52.4	0.6	10.9	0.2	10.0	0.2	79	6	27.0	0.7
12/15/14	872	109	462	5	52.6	0.8	10.9	0.2	10.0	0.2	79	6	27.0	0.6
12/15/14	872	119	464	5	52.9	0.6	11.1	0.3	10.1	0.2	80	6	26.8	0.6
12/15/14	872	145	460	4	51.8	0.6	10.8	0.3	9.8	0.2	79	6	26.4	0.5
12/15/14	872	150	464	4	52.6	0.6	11.1	0.2	10.0	0.2	79	6	26.3	0.6
12/15/14	872	160	471	6	53.3	0.6	11.1	0.3	10.1	0.2	80	6	27.0	0.6
12/15/14	872	181.5	464	5	52.2	0.6	10.9	0.3	9.9	0.2	78	6	26.2	0.5
12/15/14	872	186.5	467	5	52.9	0.7	11.0	0.3	9.9	0.2	79	6	26.3	0.5
12/15/14	872	197.5	469	5	52.8	0.6	11.2	0.3	9.9	0.2	79	6	26.0	0.6
12/15/14	872	234.5	468	4	52.5	1.0	10.9	0.2	9.7	0.2	78	6	25.2	0.6

Table 3- Pore water analyses from CAGE-14 cruise

Run Date	Core/Site	Depth (cm)	Na (mmol/L)	±	Mg (mmol/L)	±	K (mmol/L)	±	Ca (mmol/L)	±	Sr (μmol/L)	±	S (mmol/L)	±
12/15/14	873	18.5	465	6	53.8	1.1	11.1	0.3	10.4	0.2	80	7	28.4	0.6
12/15/14	873	28.5	470	5	54.0	0.6	11.4	0.3	10.5	0.2	80	6	28.1	0.6
12/15/14	873	57	465	7	53.6	0.8	11.4	0.3	10.3	0.2	79	7	27.9	0.5
12/15/14	873	66	470	5	53.9	0.9	11.5	0.3	10.3	0.2	80	7	28.1	0.6
12/15/14	873	76.5	467	6	54.0	0.5	11.3	0.4	10.3	0.2	80	6	28.2	0.6
12/15/14	873	99	466	4	53.7	0.6	11.5	0.3	10.2	0.2	79	6	28.3	0.5
12/15/14	873	108	470	4	54.0	0.6	11.3	0.3	10.4	0.2	79	6	28.6	0.5
12/15/14	873	116.5	473	4	54.4	0.7	11.4	0.3	10.4	0.2	81	6	28.9	0.6
12/15/14	873	135.5	466	6	53.5	0.8	11.2	0.3	10.3	0.2	79	7	28.4	0.6
12/15/14	873	144.5	471	4	54.3	0.8	11.4	0.2	10.4	0.2	81	6	28.6	0.5
12/15/14	873	152	474	6	54.8	0.8	11.5	0.4	10.5	0.2	81	6	28.6	0.6
12/15/14	873	174	474	8	54.4	0.8	11.6	0.3	10.5	0.2	80	7	28.5	0.7
12/15/14	873	183	469	5	53.6	0.7	11.3	0.3	10.3	0.2	79	6	28.5	0.6
12/15/14	873	192	480	5	55.0	0.6	11.6	0.3	10.6	0.2	82	6	29.5	0.6
12/15/14	874	9	466	4	53.7	0.6	11.2	0.3	10.6	0.2	79	6	29.0	0.6
12/15/14	874	34.5	475	5	54.3	0.7	11.4	0.3	10.7	0.2	81	7	29.0	0.6
12/15/14	874	57.5	475	9	54.1	0.8	11.3	0.3	10.6	0.2	80	7	28.6	0.5
12/15/14	874	130	473	5	53.8	0.7	11.2	0.3	10.4	0.2	80	6	28.1	0.6
12/15/14	874	147	468	4	53.0	0.6	10.9	0.3	10.2	0.2	79	6	27.6	0.6
12/15/14	874	167.5	474	4	53.3	0.6	11.1	0.3	10.3	0.2	79	6	27.5	0.6
12/15/14	874	183	474	4	53.6	0.9	11.1	0.3	10.3	0.2	80	6	27.4	0.7

**Methane hydrate stability and saturation in Ulleung Basin:
A numerical model perspective
(manuscript in progress)**

Malgorzata Peszynska¹, Wei-Li Hong^{2,3}, Marta Torres², and Ji-Hoon Kim⁴

¹Department of mathematics, Oregon State University, USA

²College of Earth, Ocean, and Atmospheric Sciences, Oregon State University, USA

³Center of Arctic Gas Hydrate, Environment, and Climate (CAGE), Arctic University in Norway

⁴Petroleum and Marine Research Division, Korea Institute of Geosciences and Mineral Resources, South Korea

Setting the stage

Environmental parameters of the study sites

In this effort, four sites drilled during the 2010 UBGH2 expedition in Ulleung Basin, East Sea, were chosen (Figure 1). These sites were drilled to target the blanking spots from the seismic reflection that extend to near seafloor as pockmarks or mounds (ref). These seismic blanking zones may indicate the conduit for gas migration due to the low velocity of seismic wave when encountering gas. Gas hydrates with different occurrences were recovered from all four sites. From three of the sites (UBGH2-3, UBGH2-7, UBGH2-11), massive gas hydrates, which are related to fracture filling (or grain displacing) morphology (Bahk et al., 2013), were observed at shallow depth (>6 mbsf). Disseminated gas hydrates that are related to either fracture filling or pore filling morphology were recovered from UBGH2-2_1 (Bahk et al., 2013).

Different pore water chloride profiles (Figure 2) from the four sites imply different gas hydrate kinetics and origins of the fluid. Chloride contents are always lower than seawater value at the bottom of the cores suggesting input of fresh water from clay mineral dehydration (Kim et al., 2013). Different degrees of chloride enrichment were observed from these sites. At UBGH2-3, the site with most prominent chloride enrichment, the content can be almost three times of the seawater value. At UBGH2-7 and UNGH2-11, enrichments are ~180 and few mM more than

seawater concentration, respectively. Site UBGH2-2_1, the site with strong fresh water input, no enrichments in chloride was observed. It is worth noticing that, these enrichments in chloride concentration may be affected by gas hydrate dissociation during core recovery (ref). The enrichments reported here should be considered as the minimum values; the actual magnitude may be larger. The relevant environmental parameters were summarized in Table 1.

Definitions and units

We will focus on the stability and saturation of sI hydrate with methane as the only gas component. We will therefore use methane hydrate, instead of gas hydrate, hereafter to specify the single component sI hydrate. Three phase equilibrium (aqueous-hydrate-vapor) will be computed to define the base of hydrate stability zone (HSZ). However, as our model takes into account only aqueous and hydrate phase (i.e., no multicomponent transport), the equilibrium of these two phases is more important. We consider NaCl as the only thermodynamic inhibitor. Other electrolytes such as KCl or CaCl₂ also serve as inhibitors (ref); however, due the an-order-of-magnitude higher content of NaCl comparing to other inhibitors and to simplify problem, we will primarily concern the effect from NaCl.

Salinity is one of the most fundamental parameters, along with temperature and pressure, when considering the saturation and stability of gas hydrate. Various units were adopted for salinity in the literatures which may cause some confusion and require further clarification. Absolute salinity is define as the mass fraction of dissolved salts in water (Forschhammer, 1865) (units including wt‰, wt%, g/kg, etc). This is an intuitive unit and necessary for numerical modeling which accounts for mass balance. However, it is practically impossible to precisely measure the concentration of all dissolved material (Millero et al., 2008). One alternative approach is to relate absolute salinity to chlorinity, the mass fraction of chlorine, since chlorinity can be precisely measured by titration. The internationally accepted conversion is

$$S_{ab} = 1.80655Cl_{wt} \quad (1)$$

where S_{ab} is the absolute salinity (weight fraction of salt in seawater) and Cl_{wt} is the weight fraction of all halides (mostly chlorine and bromine) in seawater.

The 1978 UNESCO *practical salinity scale*¹ (PSS-78), which expresses salinity in terms of the conductivity of water relative to the standard under fixed temperature and pressure, is the universal standard way for salinity measurement after 1978. As Millero et al. (2008) summarized, this conductivity-salinity relationship was essentially established by measuring the conductivity and chlorinity of a Standard Seawater and then convert chlorinity to salinity through

$$1.80655Cl_{wt} = S_{PSS78} \quad (2)$$

where S_{PSS78} is the conductivity-defined salinity (unitless).

For our case in Ulleung Basin, we intent to infer salinity from chlorinty (Eq. (1)) which were expressed as molarity (M), the moles of substance for a given volume of mixtures (*i.e.*, pore water). The conversion is:

$$S_{ab} = 1.80655 \times (35.453 \frac{Cl_M}{\rho_{sw}}) \quad (3)$$

where ρ_{sw} , the density of seawater, is assumed to be 1030 kg/m³, Cl_M is chlorinity in molarity. For the comparison with the values in the literatures, we will present all salinity values as the multiple of seawater salinity so that the value in any of the literature can be self-consistent.

To convert depth to corresponding pressure, we need to assume hydrostatic relationship:

$$P = \rho g(H+z) \quad (4)$$

where P is pressure in MPa, ρ is the density of seawater (1030 kg/m³), g is gravitational acceleration (9.8 m/sec²), H is water depth, and z is the depth below seafloor. The pressure at the depth of

¹ The abbreviation PSU, practical salinity unit, is a misuse. See Millero (1993) for clarification

seafloor, first gas hydrate appearance, and BSR were reported in Table 1. Between depth and sub-bottom temperature, the conversion was done by:

$$T = T_0 + Gz \quad (5)$$

where T_0 is seafloor temperature and G is local geothermal gradient (Table 1).

Saturation and Stability of Methane Hydrate

We used the theoretically calculated methane hydrate saturation (MHSAT) and stability (MHEQ) as a backbone of discussion since these calculations can be extend to the entire P-T-S regime instead of just discrete measurements or observations. It is however important to compare the theoretical calculation with experimental results. The following theoretical calculation and empirically-derived relationship will be focused. Their pressure, temperature, and salinity range and applicability is summarized in Table 2.

- Maekawa et al. (1995) fitted their lab measurements of MHEQ under different salinity conditions with the following equation:

$$\ln\left(\frac{P}{P_0}\right) = -926.815 + \frac{31979.3}{T} + 144.909\ln(T) + 5847.92x + 322.026x^2 + 5840.5\ln(1-x) \quad (6)$$

where P and P_0 are pressure in MPa at different depth and atmospheric pressure (0.101 MPa). T is temperature in K. x is the mole fraction of NaCl in the aqueous phase. This relationship can be applied to condition with salinity ~8.5 times higher than seawater value (20 wt%) and is in good agreement with other laboratory data under high salinity condition (de Roo 1983 and Kobayashi et al., 1951).

- Davie et al. (2004) use a parametric approach by fitting the theoretical calculation done by Zatsepina and Buffett (1997) to derive MHSAT. The essential equations in their work are:

$$C_3(T, P, S) = (1 - \beta S) \left[C_3(T_0, P_0, 0) + \frac{\partial C_3(T, P, 0)}{\partial T} (T - T_0) + \frac{\partial C_3(T, P, 0)}{\partial P} (P - P_0) \right] \quad (7)$$

$$C_{eq}(T) = C_3(T, P, S) \exp\left(\frac{T - T_3}{\alpha}\right) \quad (8)$$

$$C_3(T, P, S) = (1 - \beta S) C_3(T, P, 0) \quad (9)$$

$C_3(T, P, S)$ is the solubility of methane hydrate (*i.e.*, methane concentration) under at three phase equilibrium. T_0 and P_0 in Eq. (7) are the temperature and pressure of some reference state. β is a parameter determined from the theoretical calculation of Zatsepina and Buffett (1997). C_{eq} in Eq. (8) is the MHSAT within HSZ (*i.e.*, within the condition where only two phases are present). α in Eq. (8) is obtained by fitting the theoretical calculation in Zatsepina and Buffett (1997). The parameters required in Eqs. (7) and (8) are provided in Davie et al. (2004) and listed in Table 3.

- Tishchenko et al. (2005) used a semi-empirical approach based on the theoretical work by Pitzer (1991) to derive both MHEQ and MHSAT from pure water condition to salinity twice of seawater value.
- A more recent work by Sloan and Koh (2008) developed the software CSMGem, based on the models proposed by Barrer and Stuart (1957), Waals and Platteeuw (1959) and Ballard (2002), to calculate MHEQ by the statistical thermodynamic approach. The detail consideration and assumption can be found from their book.

In Figure 3, the comparisons of MHEQ under different salinity conditions estimated or measured by previous works were shown. Estimations by Maekawa et al (1995), Tishchenko et al (2005), and CSMGem are in good agreement for salinity equal or lower than seawater value. These estimations are also in agreement with other experimental results and field observations. For salinity up to double of seawater value, reduction of MHEQ estimated by Tishchenko et al (2005) is greater than that estimated by CSMGem and the empirical relationship derived by Maekawa et al. (1995).

MHSAT, or the maximum methane concentration in the H+Lw phases, under three different pressure and five salinity conditions were compared in Figure 4. Only few experimental data for

conditions with salinity higher than seawater value available (Kim et al., 2008), their accuracy is difficult to determined (Sloan and Koh, 2008). For condition with fresh water and low pressure, theoretical estimations by Tischenko et al (2008) and CSMGem agree better with each other and the experimental results. As salinity increases, both Tischenko et al. (2008) and Davie et al. (2005) suggested a reduction in MHSAT (i.e., the maximum methane concentration in equilibrium with hydrate decreases), in agreement with the laboratory results from Kim et al. (2008). CSMgem however suggests an increase in MHSAT (Figure). The theoretical calculation done by Zatsepina and Buffet (1998) also suggest an increase in MHSAT with salinity is higher than about 0.1 m. The lack of experimental data makes the evaluation of different theoretical analyses for higher salinity scenario difficult.

We implanted the MHEQ and MHSAT estimated by CSMGem in our kinetic model. To take into account the influence of salinity, we calculated the slopes between salinity and MHSAT for different pressure based on the tabulated values obtained from CSMGem (Figure 5).

Model response

We ran the model for five different scenarios (Table 4) to investigate how the profiles of dissolved methane concentration, salinity, and hydrate saturation response to the different modes of fluid transport. For the top boundary condition, we used bottom seawater salinity and methane concentration. Bottom boundary condition of methane was assumed to be equal to MHSAT at the corresponding depth. Such choice of methane bottom boundary condition confines our simulation in the phase boundary with only dissolved methane and methane hydrate. Salinity at the bottom of model was assumed to be lower than bottom seawater value reflecting the input of fresh fluid observed from our profiles (Figure 2) and by Kim et al. (2013). All the model runs were initiated without any methane in the sediments. A linear interpolation between the top and bottom salinities was assumed for the initial condition.

Comparing cases with different *Péclet* numbers (Model runs #1, #2, and #3 in Figure 6), advection effectively transports fluid with abundant methane from great depth which facilitates the formation of hydrate (Figure 6c). Hydrate saturation reaches >30% after 100 kyr of model run

with strong advection (run #3) comparing to runs with *Péclet* number smaller or equal to 1 (run #1 and #2). We noticed that, even with strong advection (*e.g.*, *Péclet* number equals to ~166 in run #3), no brine was formed at any depth in the sediments. On the contrary, due to the strong advection, the whole sediment column was flushed by the fresh water from the bottom of the model. Such result contradicts the observations from our study sites, where shallow brine coexists with the abundant gas hydrate in the sediments (Figure 2). Torres et al. (2004) concluded that methane transport exclusively by fluid phase is insufficient to sustain the hydrate formation rate required to produce the observed salinity enrichment. A different source of methane other than fluid transport is required.

In model run #4, we investigate the case with an arbitrary source of methane charges the sediments from the depth where abundant gas hydrate was observed (~17 mbsf at UBGH2-7) and with minimum advection (*Péclet* number $\ll 1$ in Table 4). In response to the strong methane input, methane hydrate saturation exceeds the highest saturation in run #4 within 5 kyr. Because of the rapid formation of methane hydrate, increasing rate in salinity at this depth exceeds the rate of diffusion and result in a patch of brine water above 50 mbsf. After running the model for 10 kyr, the hydrate saturation exceeds 60% and the salinity is 1.8 times higher than the value in bottom seawater, enrichment in salinity similar to what we observed from the profiles (Figure 6d).

In the last model run (run #5), we included both advection and the arbitrary source of methane (Table 4). Similar to the result of run #4, hydrate saturation increases rapidly around the depth where methane is injected laterally. However, the saturation is lower in run #5 as comparing to that in #4 for the same model time (*e.g.*, 10 kyr). This is because some of the methane injected is transported towards the seafloor by the strong advection. Besides, the methane hydrate in run #5 spreads in a broader range comparing to that in run #4 due to the methane brought by advection from the bottom of the model frame. The magnitude of the salinity enrichment is also smaller than that in run #4 due to the dilution by the deep fresh fluid transported by strong advection.

The explanation for the arbitrary source of methane used in the model to recreate the shallow brine patches is still enigma. As shown by Hong et al. (2014), methane production through organic matter degradation initiates at the depth where sulfate in the pore water depleted and me-

thane concentration starts to increase (*i.e.*, SMTZ). Such depth also corresponds to where the brine patches were observed in Ulleung Basin. We therefore speculate methanogenesis could be the methane source required to sustain the rapid hydrate formation as observed in our model. The range of methanogenesis rate in Ulleung Basin, as Hong et al. (2014) estimated from one chimney and one non-chimney site, is between few to ~ 25 mmol/m³/yr. By using the following unit conversion:

$$1 \frac{\text{mmol}}{\text{m}^3 \text{yr}} = 10^{-3} \frac{\text{mol}}{\text{m}^3 \text{yr}} \times 16 \frac{\text{g}}{\text{mol}} \times 10^{-3} \frac{\text{kg} (\text{CH}_4)}{\text{g}} \times \frac{1}{1030} \frac{\text{m}^3}{\text{kg} (\text{SW})} \times 1000 \frac{\text{yr}}{\text{kyr}} = 1.55 \times 10^{-5} \frac{\text{kg} (\text{CH}_4)}{\text{kg} (\text{SW}) \text{kyr}}$$

the arbitrary rate we used in model run #4 is equivalent to 5.34×10^3 mmol/m³/yr which is much greater than the rate estimated by Hong et al. (2014). This comparison suggests that the rate of methanogenesis may not be fast enough to supply the methane required to explain the rapid hydrate formation and the consequential shallow brine.

The comparison among model run #3, #4, and #5 suggests that advection can effectively transport fresh and methane-rich fluid from the bottom of model domain and facilitates the formation of methane hydrate. We however were not able to recreate the brine seen from our Cl profiles in the case with strong advection (Figure 6e). The lack of positive salinity anomaly is due to the rapid advection which delivers the fresh fluid from bottom and dilutes the hypersalinity result from the fast hydrate formation. Only when the fluid advection rate is low, as seen in our model run #4, the observed magnitude of salinity enrichment can be reproduced from our model. Unlike what was shown by Liu and Flemings (2006), both the observed profiles (Figure 2) and our model results (Figure 6d) show confined brine at shallow depth (< 50 mbsf) but not below. Liu and Flemings (2006) hypothesized that the positive salinity anomaly result from rapid hydrate formation generates a local three-phase equilibrium that allows methane gas to migrate upward and extends the saline tongue to the depth observed today. Such extended positive salinity anomaly is, however, not observed in Ulleung basin and elsewhere (Torres et al., 2011).

Figure Captions

Figure 1: Map

Figure 2: The profiles of Cl in pore water for the four study sites.

Figure 3: Methane hydrate stability (MHEQ) for different salinity, pressure, and temperature estimated by various models. Available experimental data were shown for comparison. For salinity under seawater, all models agree well with each other and the experimental data. The stability field estimated by Tischenko et al. (2005) strays away from the theoretical estimation by CSMGem and the estimation by Markawa et al. (1995) based on interpolation of experimental data.

Figure 4: Methane hydrate saturation (MHSAT) for different salinity, pressure, and temperature estimated by various models. Only few experimental data for pure water and 2x seawater conditions are available for comparison. The saturation estimated by CSMGem is always higher than the one estimated by Davie et al. (2004) while the saturation estimated by Tischenko et al. (2005) overlaps with one or the other depends on salinity. Lack of constraint from experimental data makes the justification of different theoretical estimation difficult.

Figure 5: The slope (α) between salinity and MHSAT at different salinity, temperature, and pressure estimated from the tabulated value calculated by CSMGem. The positive α suggests that methane hydrate is more difficult to form when the salinity is higher. Higher temperature also elevates MHSAT and makes methane hydrate more difficult to form. MHSAT slightly decreases when applying more pressure under the same temperature and salinity.

Figure 6: Model results of the five runs. Parameters for each model run can be found in Table 4. The observed salinity enrichment can be reproduced in model run #4 by adding an arbitrary source of methane. See text for more details about the results of each model run.

Table 1 Basin parameter of the four study sites in Ulleung Basin

	UBGH2-2_2	UBGH2-3	UBGH2-7	UBGH2-11
Water depth (m)	2093	898	2145	2082
P at seafloor (MPa) ^a	21.13	9.06	21.65	21.02
Seafloor temperature (K) ^b	273.35	273.45	273.55	274.35
BSR depth (mbsf)	180.5	131.6	124	159
P at BSR (MPa) ^a	22.95	10.39	22.90	22.62
BSR temperature (K) ^c	292.7	286	294.8	292.2
First hydrate appearance depth (mbsf) ^d	67.9	6.2	7	7
P at 1 st GH (MPa) ^a	21.81	9.13	21.71	21.09
1 st GH temperature (K) ^c	273.4	274	274.6	275.1
Geothermal gradient (°C/m) ^e	0.107	0.095	0.171	0.120
Salinity at BSR (kg/kg)	1.44E-2	2.94E-2	2.50E-2	1.73E-2

^a Pressure was calculated assuming 1030 kg/m³ for seawater density and 9.8 m²/sec for gravitational acceleration.

^b seafloor temperature was measured at each of the drilling site (Lee et al., 2013).

^c temperature is estimated from seafloor temperature and geothermal gradient

^d The depth of hydrate first appearance was determined by either visual observations of hydrate of pore water anomalies.

^e geothermal gradient determined from linear regression of downhole temperature measurements at all UBGH2 drill-sites (Riedel et al., 2013).

Table 2

	Stability	Saturation	P range (MPa)	T range	S range	note
(1) Maekawa et al. (1995)	v	x	Up to 18	Up to 290	0-20 wt%	Experimental data
(2) Davie at al. (2004)	x	v	10-30	273-300	0 to seawater	Parametric approach
(3) Tishchenko et al. (2005)	v	v	Up to 50	273-297	0-70	Semi- empirical approach
(4) Sloan and Koh (2008)	v	v	?	?	?	

Table 3 Parameters required in Eqs. (7) and (8) to calculate methane hydrate stability and saturation following the Davie et al. (2004) approach.

Parameters	T_0	P_0	α	β	$C_3(T_0, P_0, S)$	$\frac{\partial C_3(T, P, 0)}{\partial T}$	$\frac{\partial C_3(T, P, 0)}{\partial P}$
Values suggested by Davie et al. (2004)	292 K	20 MPa	14.4 °C	0.1 mol ⁻¹	153.36 mM	6.34 mM/K	1.11 mM/MPa

Table 4 Parameters of the five model runs

Run #	Diffusion rate (m ² /yr)	Advection rate (m/yr)	<i>Péclet</i> number	Methane production rate (kg/kg/kyr) ¹	Model time length (kyr)
1	3E-2	1.2E-9	<<1	0	25, 50, 100
2	3E-2	2E-4	~1	0	25, 50, 100
3	3E-2	2E-2	~166	0	2.5, 10, 25, 100
4	3E-2	1.2E-9	<<1	8.3E-2	2.5, 5 10
5	3E-2	2E-3	~16.6	5E-2	10, 50, 100

¹kg of dissolved methane in per kg of seawater for every thousand years

Figure 1. Site locations

Figure 2

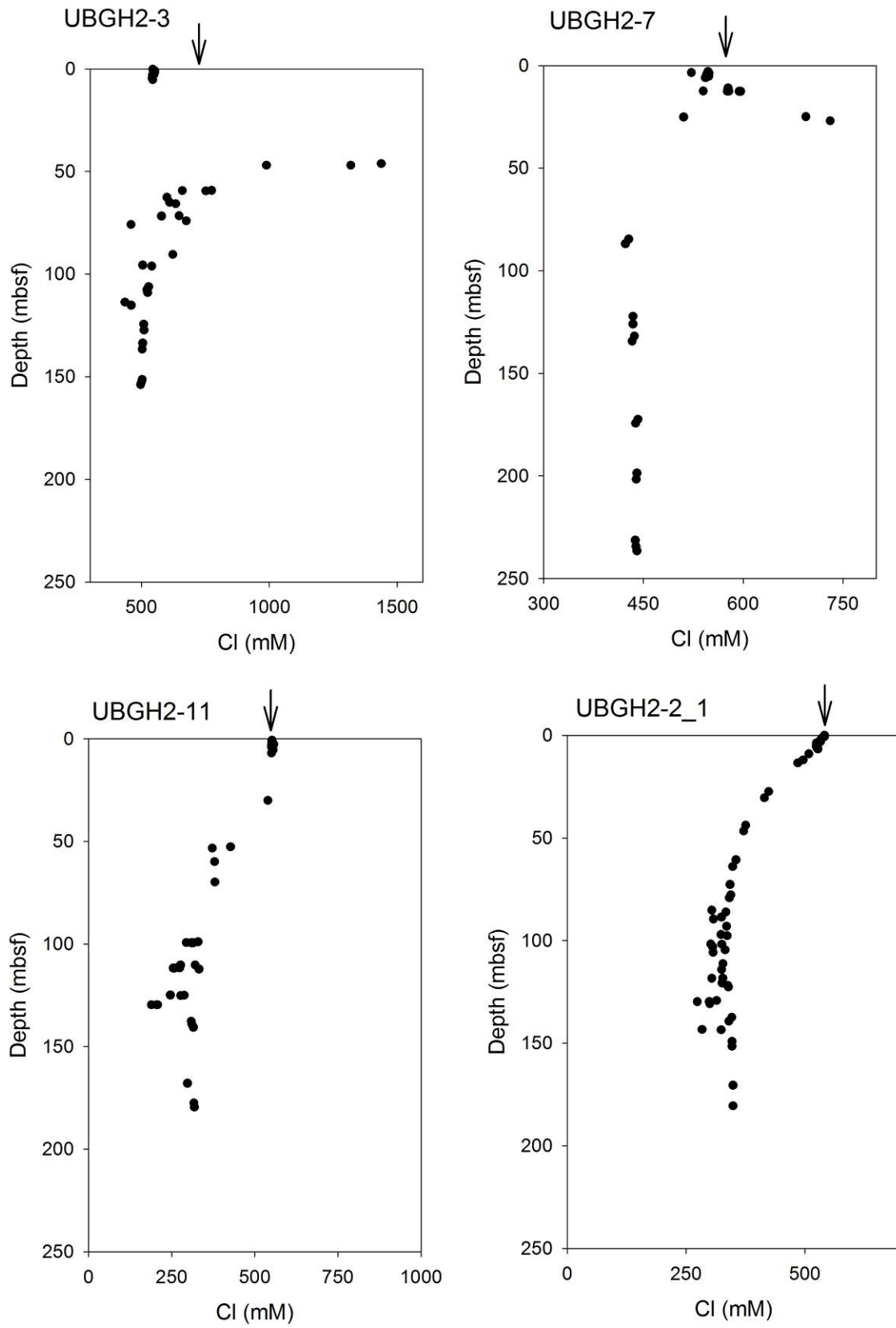


Figure 3

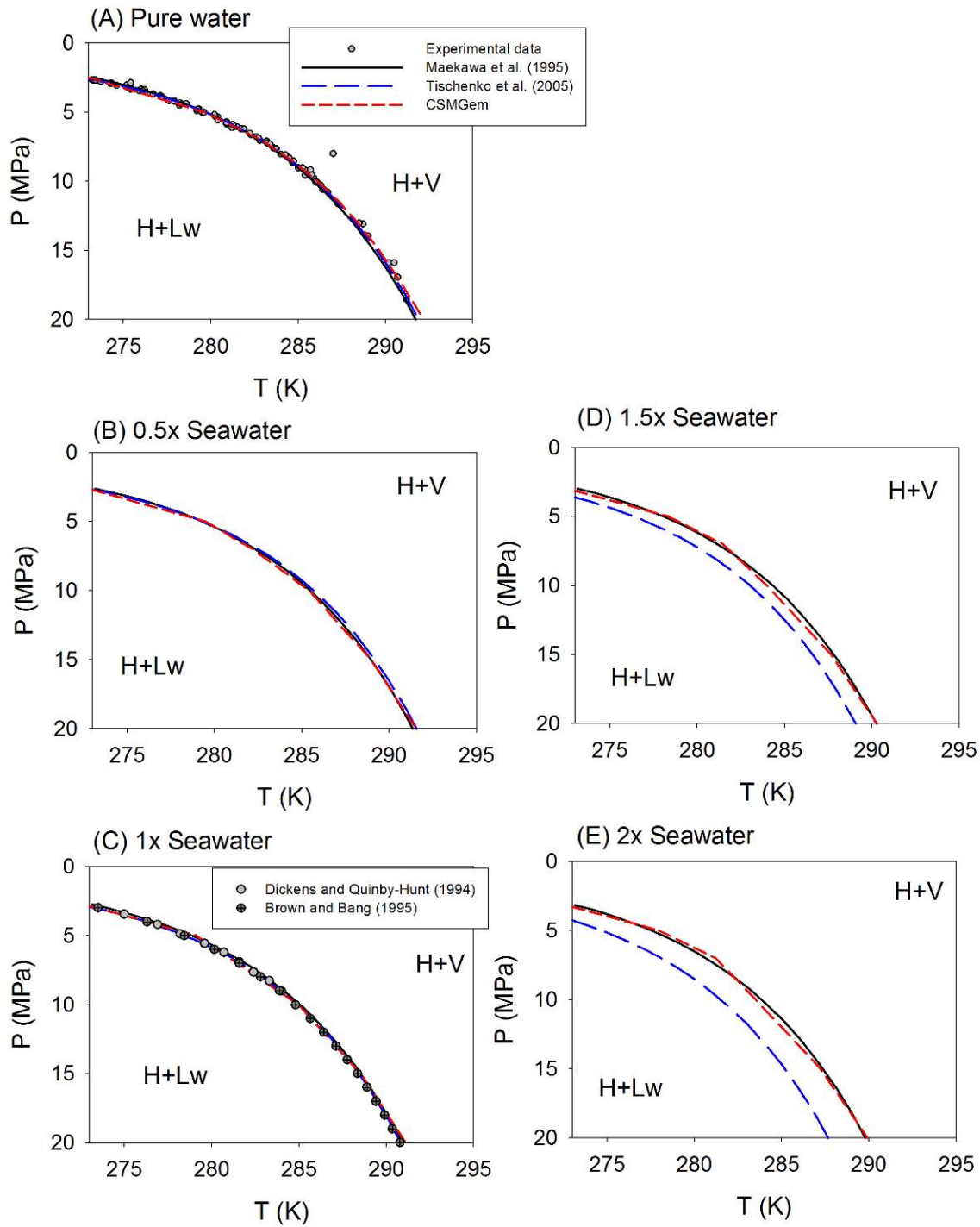


Figure 4

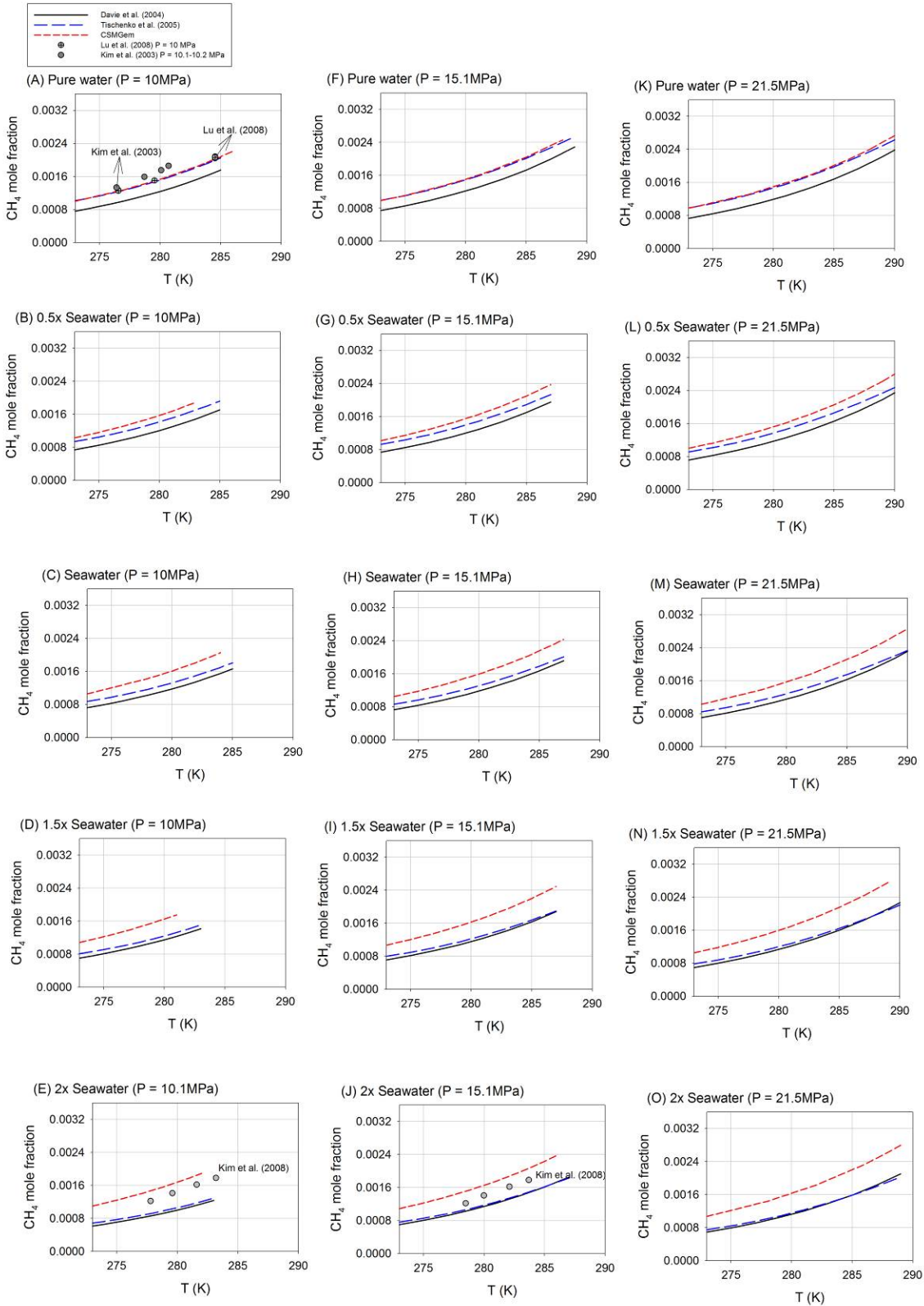


Figure 5

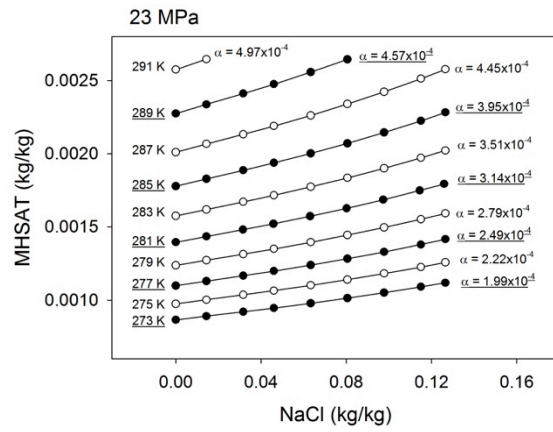
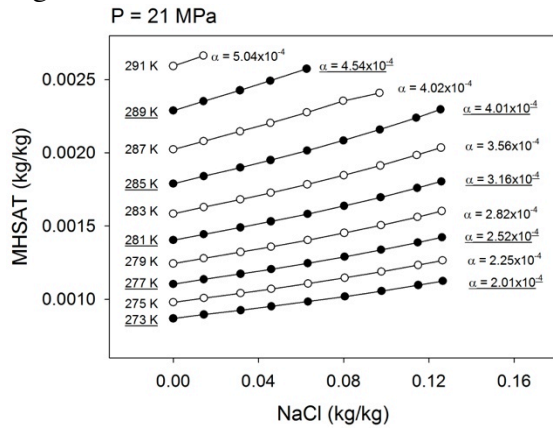


Figure 6a

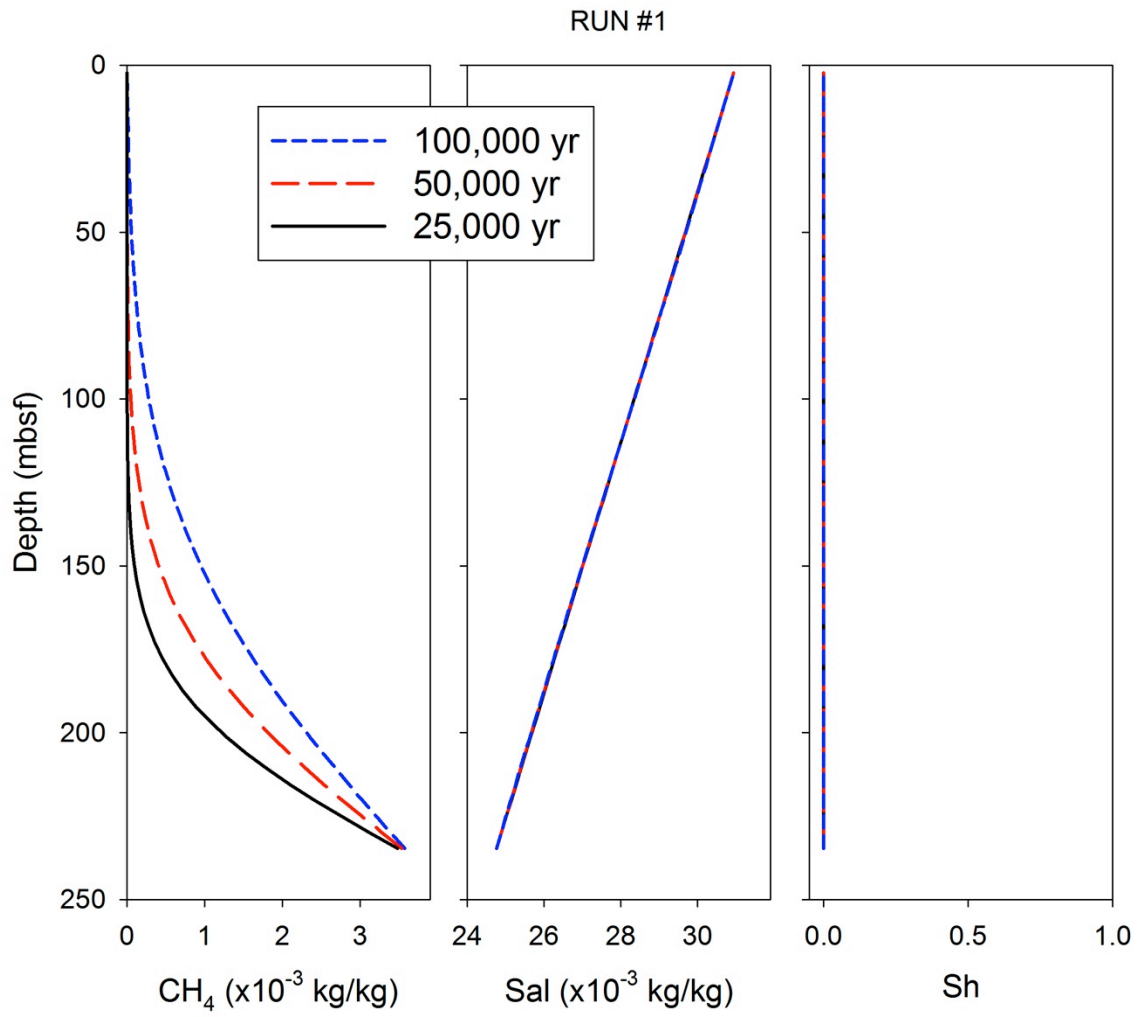


Figure 6b

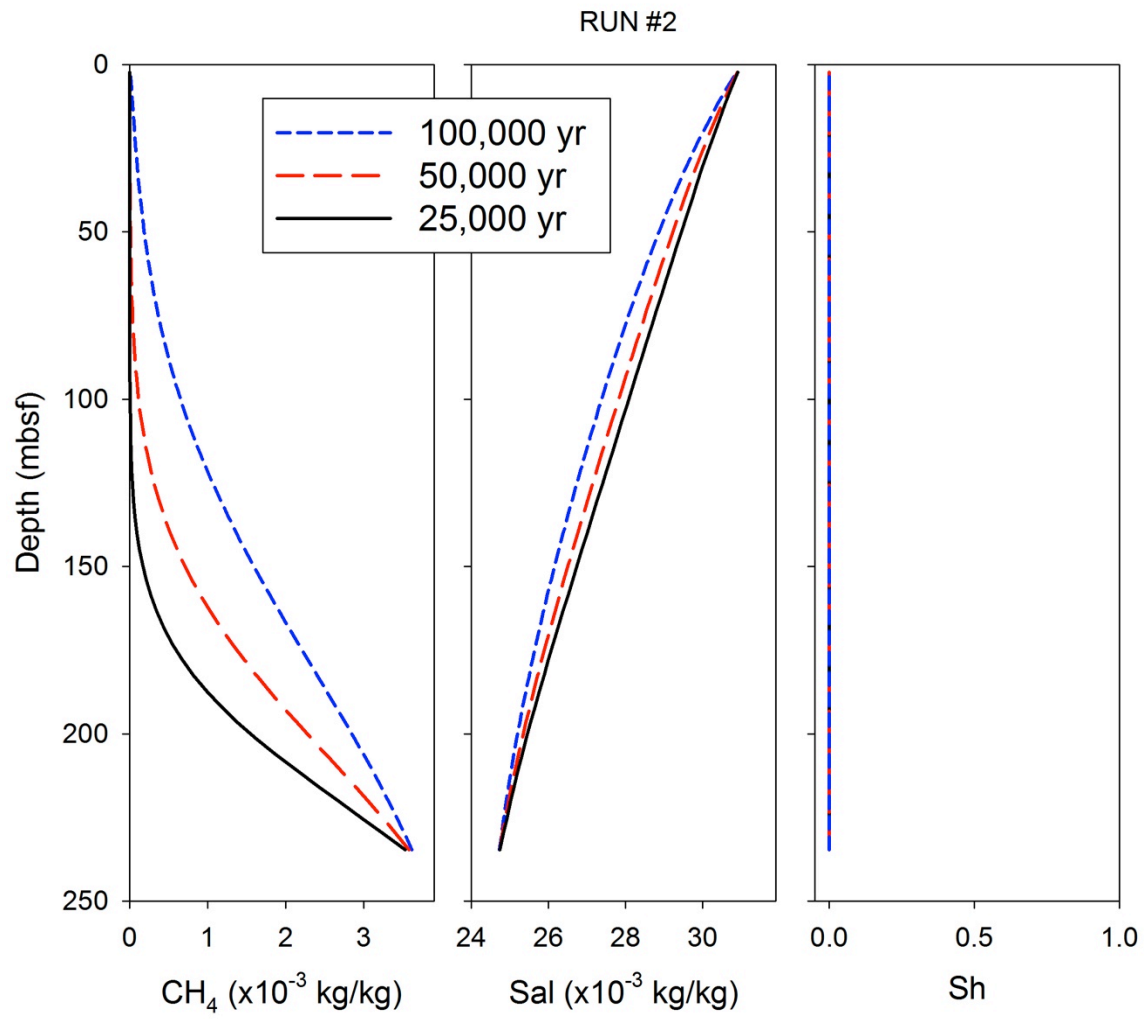


Figure 6c

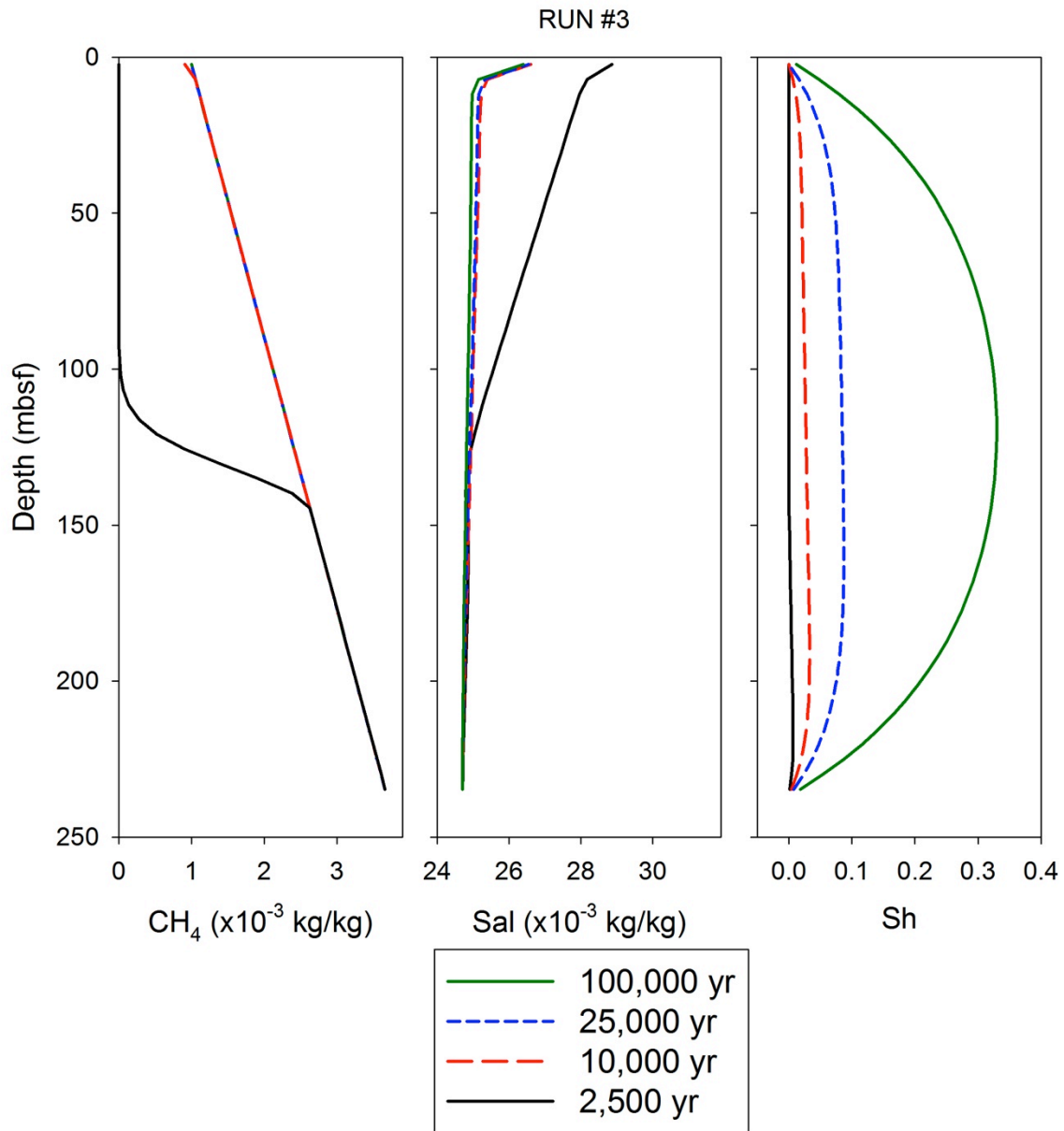


Figure 6d

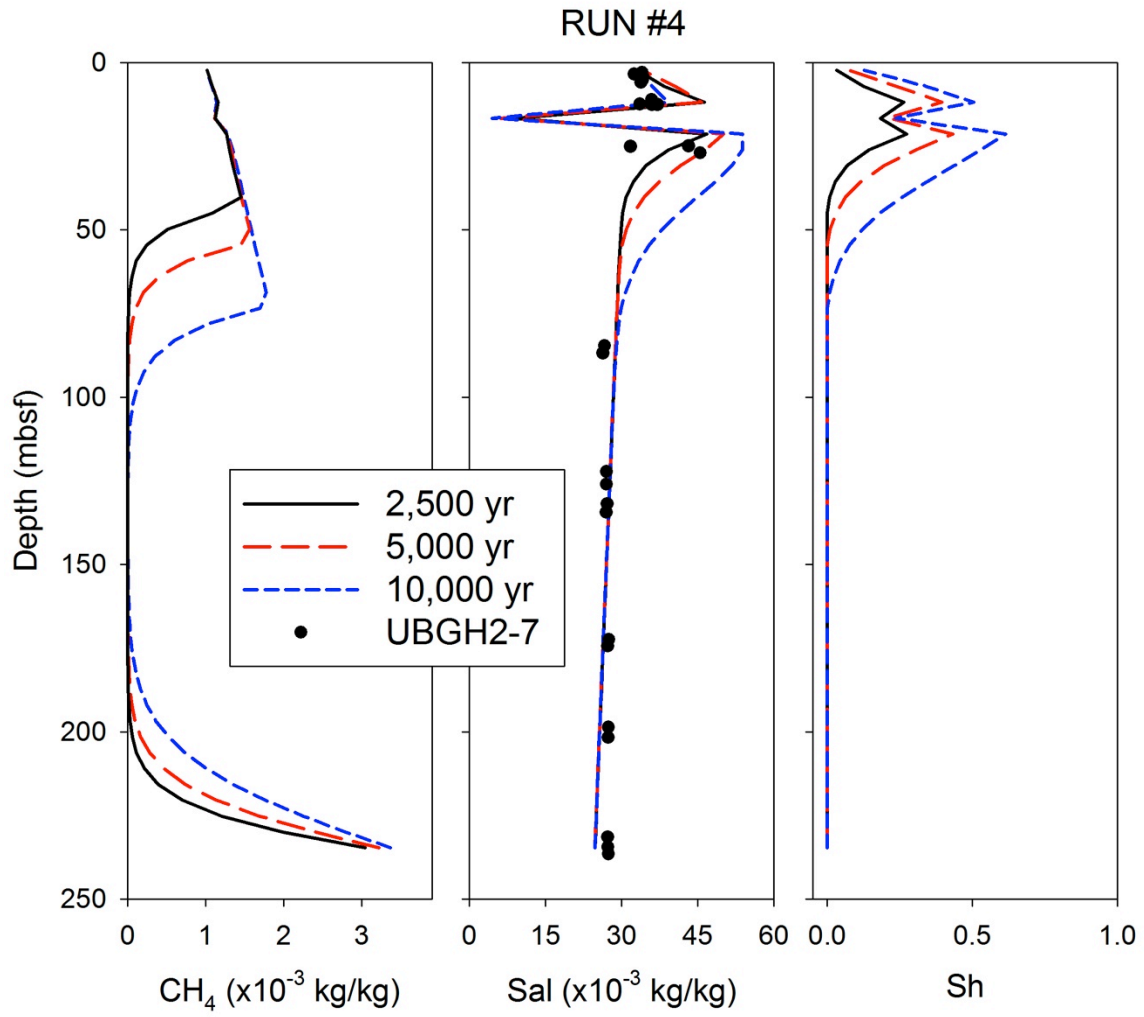
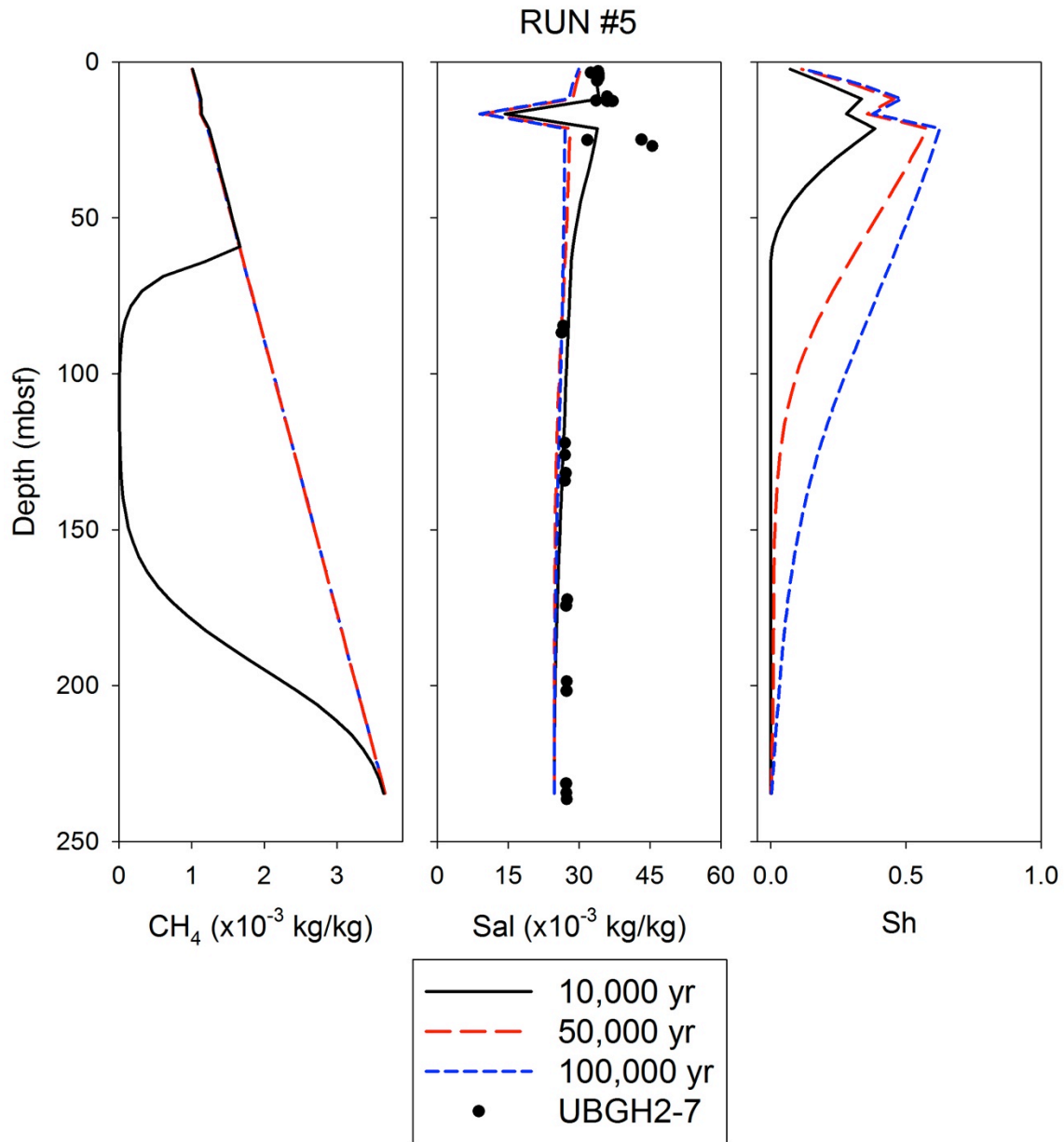


Figure 6e



National Energy Technology Laboratory

626 Cochrans Mill Road
P.O. Box 10940
Pittsburgh, PA 15236-0940

3610 Collins Ferry Road
P.O. Box 880
Morgantown, WV 26507-0880

13131 Dairy Ashford, Suite 225
Sugarland, TX 77478

1450 Queen Avenue SW
Albany, OR 97321-2198

2175 University Ave. South
Suite 201
Fairbanks, AK 99709

Visit the NETL website at:
www.netl.doe.gov

Customer Service:
1-800-553-7681

